20th AIAA Aerodynamic Decelerator Systems Technology Conference and Seminar
4 - 7 May 2009, Seattle, Washington

AIAA 2009-2942

Parachute Drag Area Using Added Mass as Related to Canopy Geometry

Brook A. Kidane*
Airborne Systems North America, Santa Ana, California, 92704

This paper presents a more accurate approximation of the mathematical relationship between riser tension and parachute drag area during inflation than is typically used in the reduction of test data to obtain important parachute performance characteristics. Drag area time history and related characteristics, such as inflation parameters, are derived from measurements of tension in the parachute-payload connection, of dynamic pressure, and of position. Typically, to form the relationship between the measured values and drag area, the tension measurement is assumed to be equal to the drag force of the parachute and, subsequently, to the product of drag area and measured dynamic pressure. Through this relationship the drag area is determined as the quotient of the riser tension and the dynamic pressure. This paper presents the actual relationship including terms for the apparent mass and the time rate of change of the apparent mass, the difficulty in the determination of which is most likely the primary deterrent in using a more complete formulation of drag area and other parameters. This challenge is addressed in this paper by relating the apparent and added mass to the inflating parachute geometry and to the freestream velocity. The basis by which this is done is reviewed, values of apparent and added mass for a specific test are computed, and comparisons of drag area determined by the typical relationship and the more exact relationship are made.

Nomenclature

Symbols

a	=	acceleration
A_j	=	acceleration vector or tensor
A_{jk}	=	apparent mass tensor
C_DS	=	drag area of parachute
D_P	=	drag force parachute
F	=	force
F_T	=	riser tension
m_A	=	added mass of parachute
m_I	=	included mass of parachute
M_{ij}	=	apparent mass matrix or tensor
m_p	=	mass of parachute
q	=	dynamic pressure
T	=	kinetic energy
U, U_i	=	freestream velocity, component of freestream velocity
u_i, u_{ij}	=	component of fluid velocity
v_p	=	velocity of parachute
V	=	volume of pressurized region of parachute
W_P	=	weight of parachute
x_i	=	component of Cartesian coordinate system
γ	=	flight path angle
ϕ	=	velocity potential function
ρ	=	density

Acronyms

TMS	=	Tension Measurement System

---

* Design Engineer, Airborne Systems North America, 3000 Segerstrom Ave, Santa Ana, CA 92704.

I. Introduction

Common procedures for producing parachute inflation characteristics and simulation input parameters rely on a simplified relationship between the parachute drag area, C_DS, and test measured forces, F_T, in the parachute-payload connection and test measured dynamic pressure, q. This simplification is legitimate in that the determination of the additional values required to formulate a more exact determination of drag area growth may not be practical when considering the needs of customers and the objectives of projects. However, in the interest of gaining knowledge on parachute inflation, a method of determining a more exact value of drag area may be pursued. Such a pursuit may be valuable in that a more accurate formulation between drag area and riser tension, with values measured during testing, may be used to determine important parachute parameters, such as those characterizing inflation, required to model performance.

II. Common Method Relation

The relation that is commonly used to determine the drag area profile is based on the approximating assumption that the riser tension is equal to the parachute drag force -- $F_T = D_P$ -- and substituting F_T for D_P in $D_P = C_D S \cdot q$ assumption resulting in the following relation.

$$C_D S = \frac{F_T}{q} \tag{1}$$

The riser tension, F_T, is measured by various methods, including by means of a Tension Measurement System (TMS), at one or more locations in the connection between the parachute and the payload. The dynamic pressure q is measured at the payload location using a pitot tube.

III. Refined Method Relation

The parachute – payload system can is described by two coupled equations of motion, one for the payload and one for the parachute. These equations are as follows:

$$\frac{d}{dt}\left[(m_A + m_p)v_p\right] = D_p - W_P \sin\gamma - F_T \tag{2a}$$

$$\frac{d}{dt}\left[(m_v)v_v\right] = F_T + D_v - W_v \sin\gamma \tag{2b}$$

A higher fidelity relation between the drag area and the measured riser tension is obtained, without any assumptions, from Eq. (2a). If riser tension is isolated in Eq. (2a), the following equation is obtained.

$$F_T = D_p - (m_A + m_p)a_p - \dot{m}_A v_p - W_P \sin\gamma \tag{3}$$

Substituting $C_D S \cdot q$ for D_P and solving for $C_D S$ the actual relationship between parachute drag area and riser tension is

$$C_D S = \frac{F_T}{q} + \frac{(m_A + m_p)a_p}{q} + \frac{\dot{m}_A v_p}{q} + \frac{W_P \sin\gamma_p}{q}. \tag{4}$$

All of the values on the right side of Eq. (4) are measured directly in a test except the added mass and the time rate of change of the added mass, m_A and $\dot{m}_A$ respectively. The added mass, m_A, appearing in Eqs. (2) – (4) is the sum of the included mass, which is the mass of air captured inside the canopy, and the apparent mass, which accounts for the force on the parachute due to the change in momentum of the fluid caused by the motion of the parachute. Some formulations treat the apparent mass and the included mass separately, but here these quantities are treated together as $m_A = m_I + m_a$ [1] where the first term in the sum is the included mass –

$$m_I = \rho V \tag{5}$$

and the second term is the apparent mass.

IV. Determining Apparent Mass

The determination of the apparent mass component of the added mass is a more complicated process. There are two general classes of methods of approximating this value. The methods of the first class relate the apparent mass to a non-dimensional coefficient, usually termed the apparent mass coefficient, and the geometry of the body in the fluid; occasionally, the volume of the body is considered specifically important as opposed to the general geometry of the body and its relationship to the flow, however Ref. 2 suggests that this is coincidental. The methods of the second class relate the apparent mass to the potential flow around the body and the geometry of the body.

Here, the methods of the second class are used as described in Ref. 2 using the primary formulations of Refs. 4 and 5. A summary of the steps required to formulate the apparent mass expression using the second method are as follows; a more complete review of the steps appears in the appendix. First, the kinetic energy of the flow around the ellipsoid is expressed in terms of the potential flow velocities around an ellipsoid approximating the instantaneous shape of the pressurized region of the inflating canopy. Second, the apparent mass is factored from this expression and expressed in terms of the velocity potential. Third, the potential function is determined, where this potential function is solely dependent on the geometry of the body[3-4] – in this case the ellipsoid approximating the instantaneous shape of the inflating canopy – and the body free-stream velocity. This will in turn give the apparent mass in terms of the body geometry. The time rate of change of the apparent mass is also expressible in terms of the body geometry. Both of these values can then be substituted in Eqs. (2), (3), and (4).

The result of these steps is an expression for the apparent mass associated with the motion of a parachute moving solely along its body fixed x_3 or z axis which is[†]

$$A_{33} = \frac{\rho\alpha_0}{2-\alpha_0}\frac{4}{3}\pi abc, \tag{6}$$

where a, b, and c are the ellipsoid dimensions in the body fixed x_1 or x, x_2 or y, and x_3 or z axis respectively and α_0 is a term appearing from the solution of the potential flow as described in the appendix. With the determination of the apparent mass as given by Eq. (6), the added mass can be expressed as

$$m_A = \frac{\rho\alpha_0}{2-\alpha_0}\frac{4}{3}\pi abc + \rho\frac{4}{3}\pi abc, \tag{7}$$

where the first term in the sum is the apparent mass and the second term is the included mass.

[†] The derivation of this expression is based on Refs. 2-5. The steps -- taken from these references -- required in determining this expression are summarized in the appendix.

V. Measurements from Drop Test Videos

The parachute used to compare the two methods of determining the drag area history was a 116 ft D_0 quarter-spherical ringsail with two stage reefing weighing 185 lb. Drop test instrument data and video was available for this parachute as part of development testing. The first data point collected for the purpose of this paper occurred immediately after the beginning of first stage inflation at an altitude of 5500.5 ft above mean sea level at and at a dynamic pressure of 42.25 lb/ft^2. Plots of test determined values used in Eq. (4) – riser tension, velocity, flight path angle, and dynamic pressure are presented in Figs. 1 – 4.

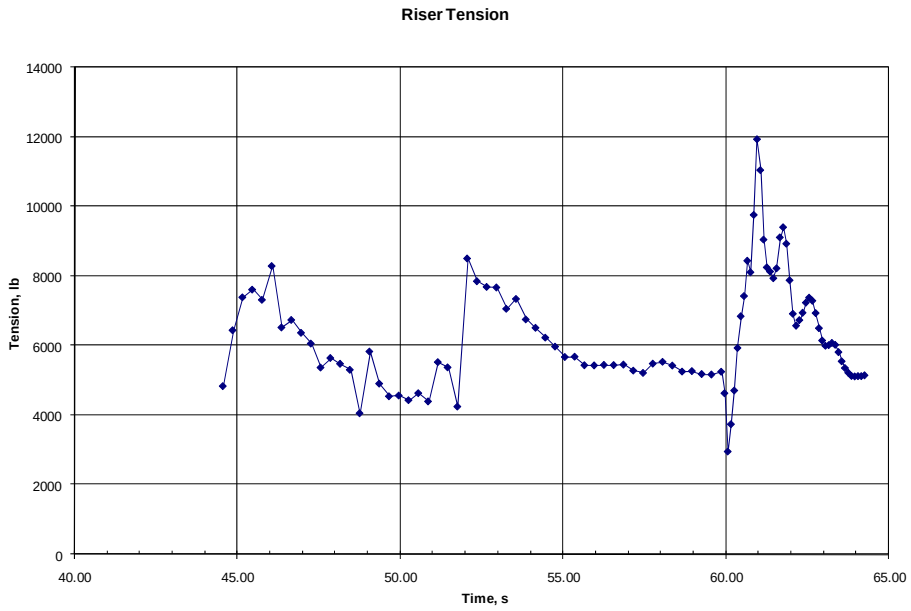

Figure 1. Riser tension measured during test. *This figure presents the measured tension from the start of inflation through full open. This is the F_T used in Eqs. (1) and (4).*

Measurements of the radial dimensions of an ellipsoid -- symmetric about the minor axis -- approximating the instantaneous shape of the pressurized region of the canopy were taken from still frames extracted from the available video. Ninety-six frames, the first of which occurred immediately after the start of inflation and the last of which occurred at full open, and

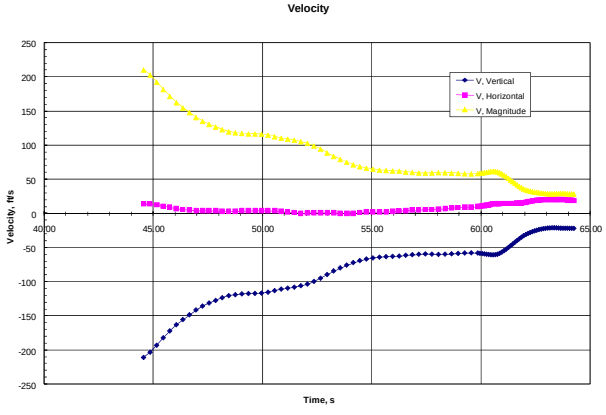

Figure 2. Velocity measured during test. *This curve presents the wind corrected velocities measured during the test. The velocity magnitude is used in Eq. (4).*

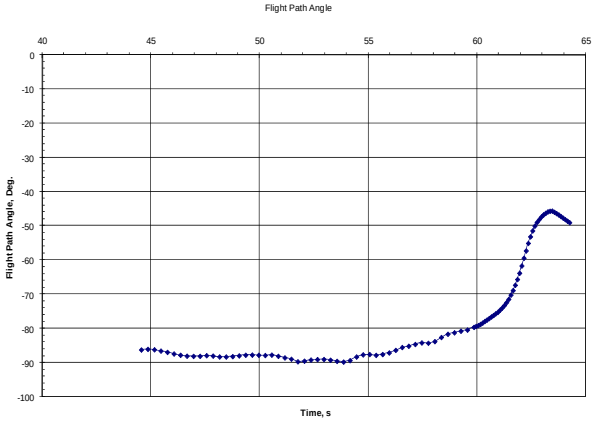

Figure 3. Flight path angle. *This curve presents the flight path angle as calculated from wind corrected horizontal and vertical velocities.*

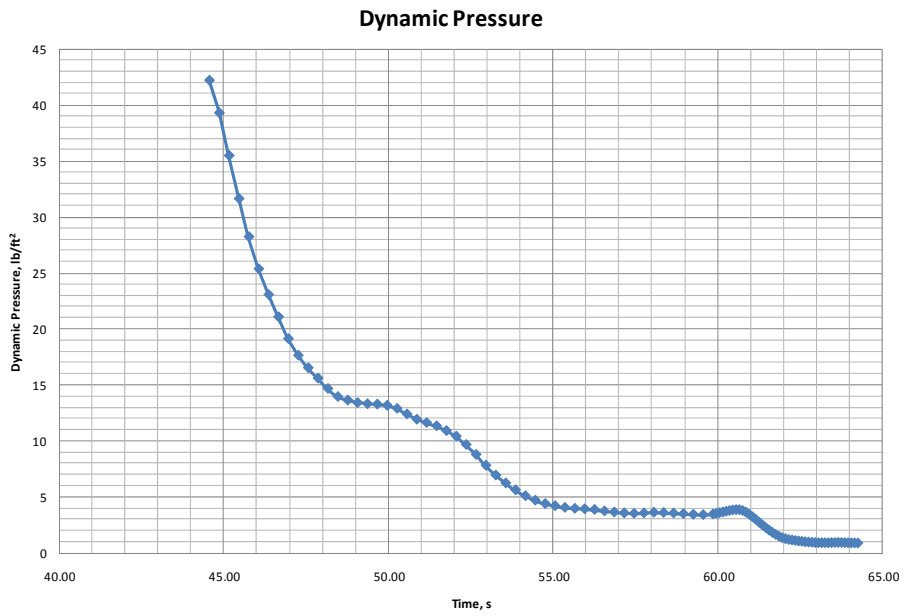

Figure 4. Dynamic pressure. *This curve presents the dynamic pressure measured during the test. It is used in Eqs. (1) and (4).*

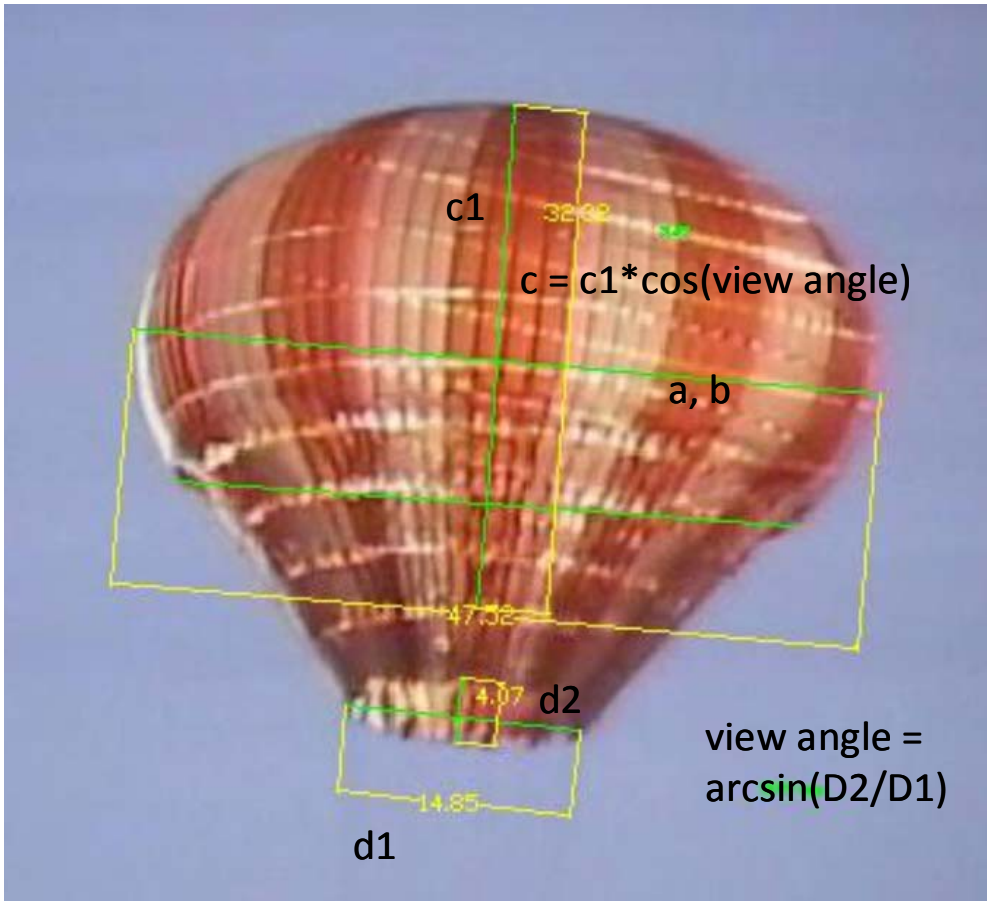

Figure 5. Sample frame extracted from video showing measurements.

intermediate frames -- at 0.33 sec intervals between inflation start and disreef to full open and at 0.11 sec intervals between disreef to full open and full open -- were examined to obtain the dimensions.

Figure 5 presents a sample frame indicating the dimensions of the ellipsoid radii, where c is the ellipsoid radial dimension coincident with the body fixed x_3 or z axis which is along the parachute axis of symmetry, and a and be are the other two dimensions which are assumed to be equal to each other. These ellipsoid radial dimensions are presented in Fig. 6. The computed volume of the ellipsoid is also presented in Fig. 6, where the volume is $V = \frac{4}{3}\pi abc$.

This time history of the ellipsoid radii and the dependent volume depicted in this figure clearly represents the growth of the canopy between start of inflation and full open – the radius, c, represents the growth less distinctively than the

radii a and b and the volume, especially at disreef to the second reefing stage, but taken together with a, b, c, and the

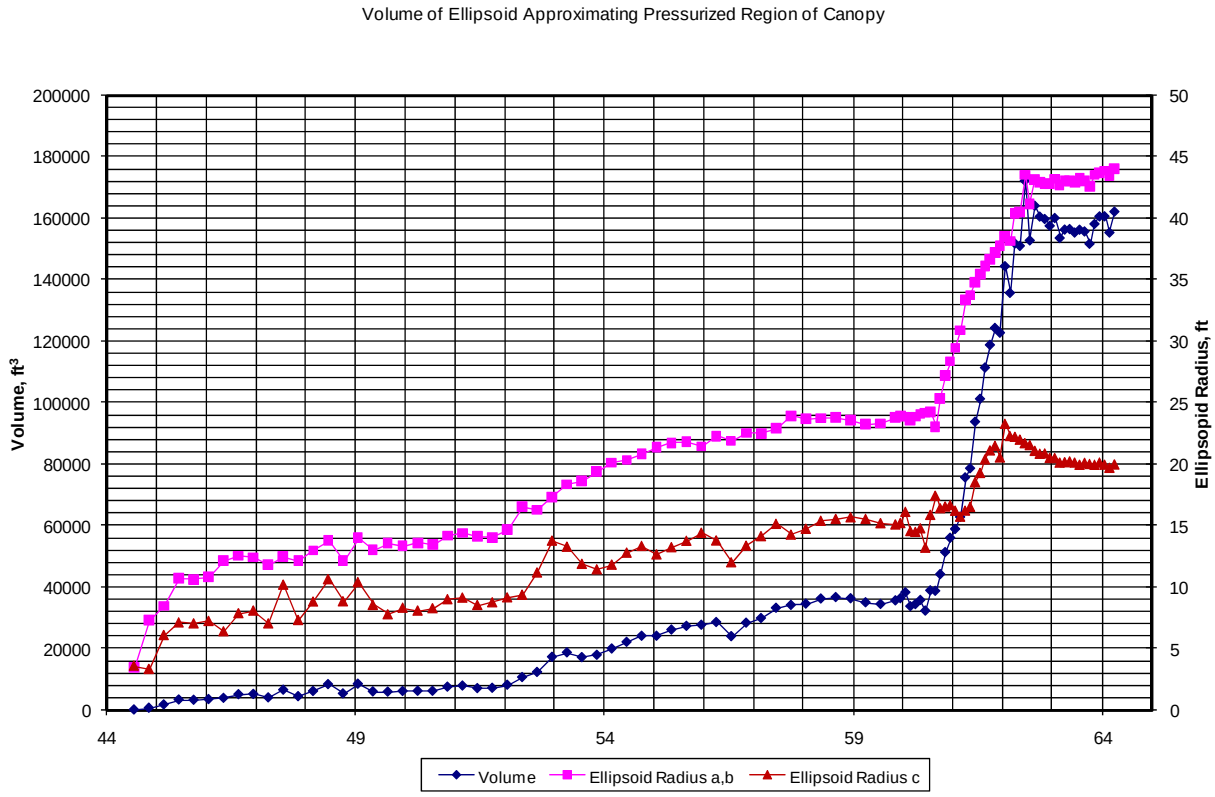

Figure 6. Ellipsoid radial dimension measurements and ellipsoid volume as a function of time between inflation start and full open. *The curve labeled Ellipsoid Radius a, b is the major axes radial dimension. a is along the x axis, b is along the y axis and c is along the z axis. Since the canopy is symmetrical about the z axis, a and be are equal.*

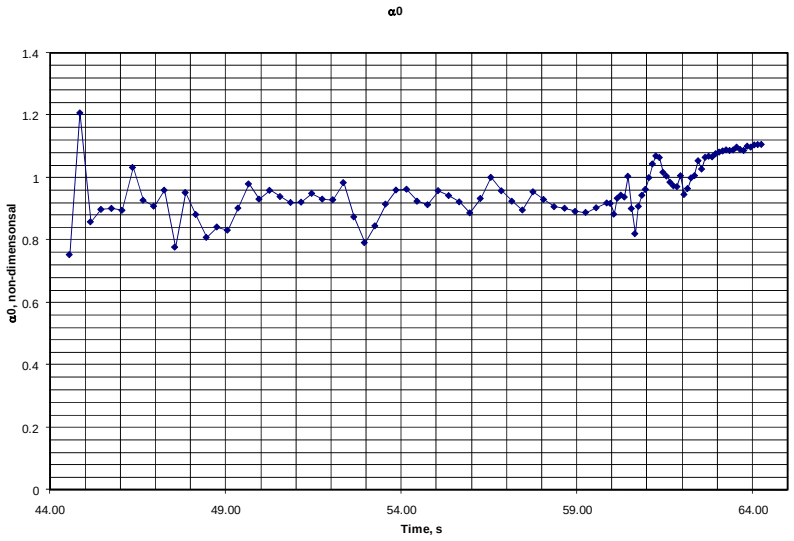

Figure 7. Values of α_0 from inflation start through full open. *These values were computed numerically from the elliptic integral appearing in the potential flow solution of flow around an ellipse.*

volume, the reefing stages can be discerned.

The value of α_0 at each data point was calculated numerically from the radii of the ellipsoid as given by Eq. (30); these values are presented in Fig. 7. The radii and α_0 values at each data point, along with velocity and density data measured by test instruments, when inputted in Eq. (6) give the apparent mass of the parachute as approximated by the ellipsoid at each point. The added mass, the sum of the apparent mass and included mass – as given by Eq. (5), was then calculated for each data point. The time history of the added mass and the apparent mass between inflation start and full open

is presented in Fig. 7.

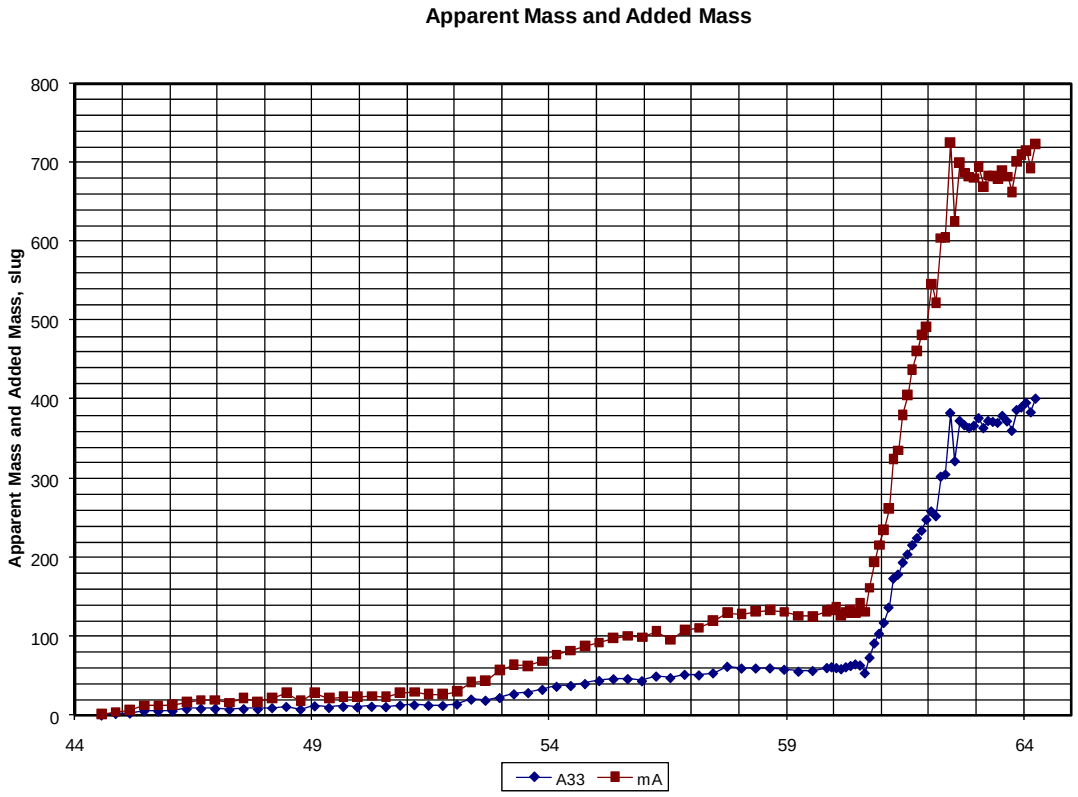

Figure 8. Apparent mass and added mass between the start of inflation and full open.. *Disreef to full open occurs at 60.65 s. Full open occurs at 62.45 s.*

This figure, as does Fig. 6, depicts clearly the growth of the canopy during the first reefing stage beginning at 44.5 s, disreef at 52 s, the moderately increased growth rate during the second reefing stage until disreef to full open, the drastically increased growth rate during inflation to full open at 60.5 s, and the subsequent constant value of the apparent and added mass – all as would be expected.

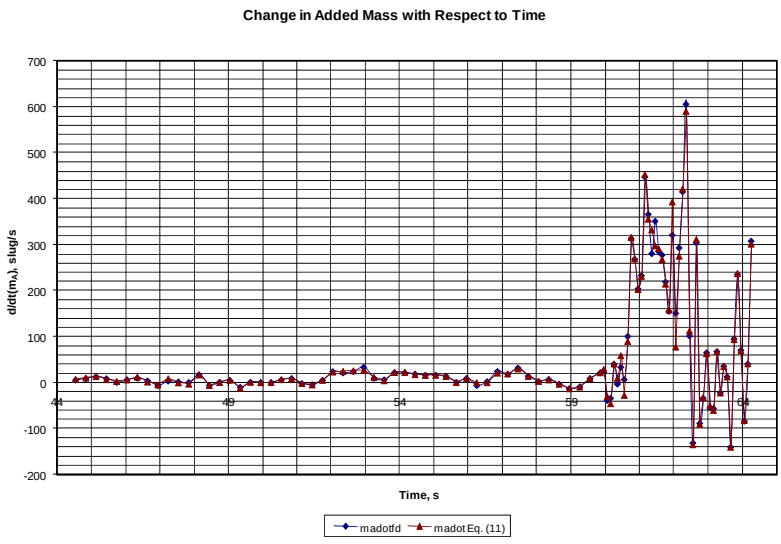

Figure 9. Added mass time derivative from inflation start through full open inflation. *The curve labeled madotfd is a finite difference of the added mass whereas the curve labeled madotEq. (11) is calculated by Eq. (11) where only the ellipsoid dimensions and L are finite differenced.*

In addition to the values presented in Figs. 6 – 8, the other component of Eq. (4) that is not directly measured by test instruments necessary to compute the drag area growth during inflation is the change in added mass with respect to time, $\dot{m}_A$. This derivative is represented by the following equation:

$$\dot{m}_A = \frac{d}{dt}\left(\frac{\rho\alpha_0}{2-\alpha_0}\frac{4}{3}\pi abc + \rho\frac{4}{3}\pi abc \right) \tag{8}$$

where the first element of the sum is the apparent mass and the second is the included mass. If the density is assumed to be constant, Eq. (8) reduces to

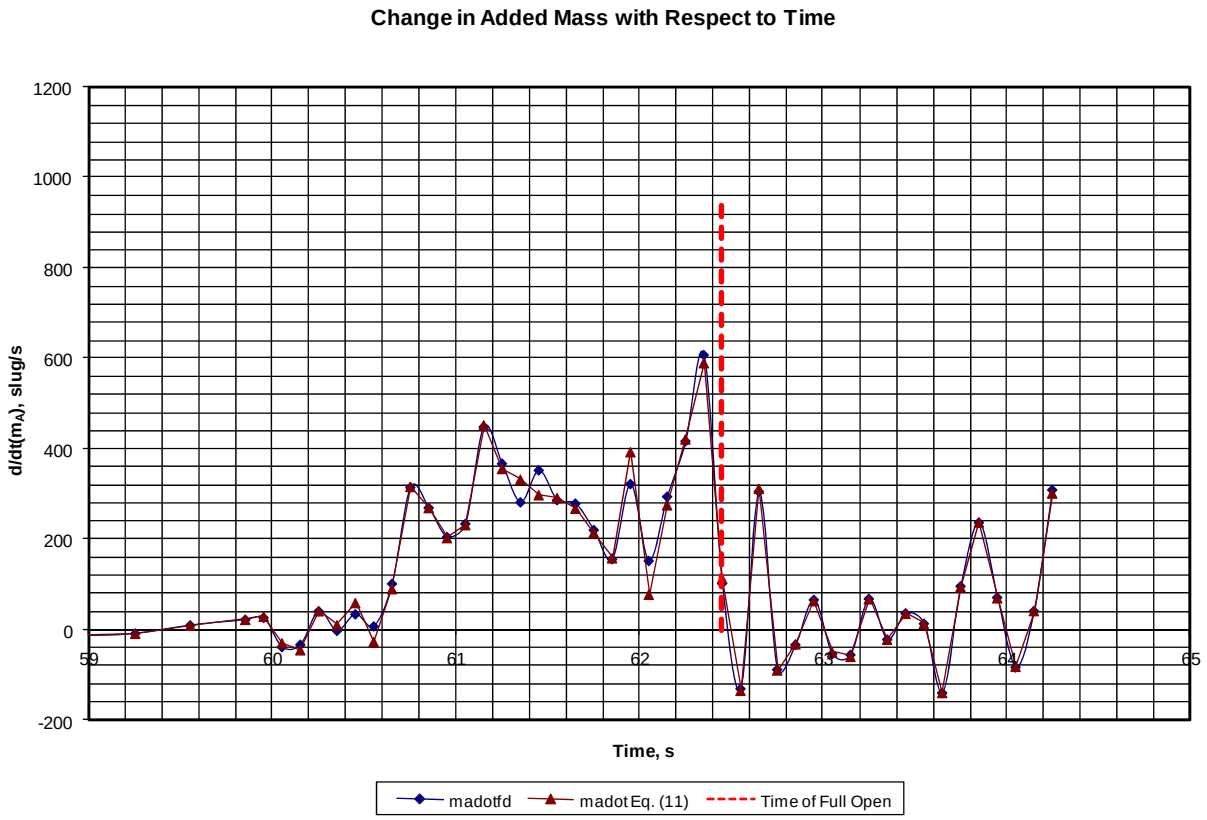

Figure 10. Added mass time derivative after disreef from second stage. *The curve labeled madotfd is a finite difference of the added mass whereas the curve labeled madotEq. (11) is calculated by Eq. (11) where the ellipsoid dimensions and L are finite differenced.*

$$\dot{m}_A = \rho\frac{4}{3}\pi \cdot \frac{d}{dt}\left(\frac{2abc}{2-abcL} \right) \tag{9}$$

where L is equal to the elliptic integral of Eq. (30) or,

$$L = \frac{\alpha_0}{abc} \tag{10}$$

Eq. (9) is also expressible as

$$\dot{m}_A = \frac{\rho}{(2-abcL)}\frac{4}{3}\pi\left[\frac{d}{dt}(a)bc + a\frac{d}{dt}(b)c + ab\frac{d}{dt}(c)\right] + \frac{\rho}{(2-abcL)^2}\frac{8}{3}\pi\left[\frac{d}{dt}(a)bcL + a\frac{d}{dt}(b)cL + ab\frac{d}{dt}(c)L + abc\frac{d}{dt}(L)\right] \quad (11)$$

-- a form of the equation where the individual geometry related terms can be finite differenced separately.

The time history of $\dot{m}_A$ computed by two different methods— one by taking the average of the forward and backward finite difference of the added mass at each data point and another by Eq. (11) where the finite difference of a, b, c, and L are done separately as they appear in the equation -- is presented in Figs. 9 and 10. Both time histories show that the change in added mass is nearly constant during the first and second reefing stage, and that there is an increase in the rate that added mass changes after disreef to full open and a fluctuation centered on 0 slug/s after full open is reached.

Figures 8 - 10 indicate that the added mass and added mass change rate values are small during the first and second reefing stages compared to the period of inflation to full open. This is a direct consequence of the much larger dimensions of the canopy during the growth to the last stage resulting in higher values at that stage. The higher dynamic pressure in the first stage when the canopy is smaller also results in smaller added mass and added mass change rate during the first stage relative to the last stage inflation.

VI. Comparison of Effects of Approximate Relationship vs. Refined Relationship

The values that depend on the dimensions of the approximating ellipsoid, having been determined by Eqs. (7) and

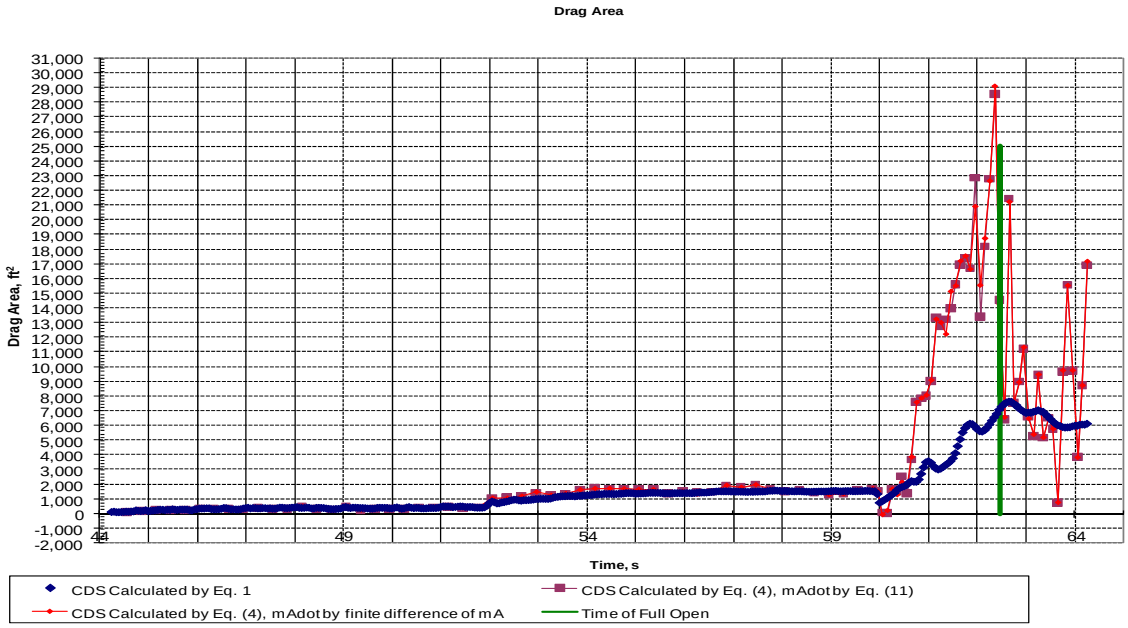

Figure 11. Drag area from the start of inflation through full open..

(11), can be inputted into Eq. (4) and the drag area values at each point can be determined. Figures 11 – 14 present the drag are time history given by Eq. (4) based on the two computations of $\dot{m}_A$ as well as the drag area given by Eq. (1).

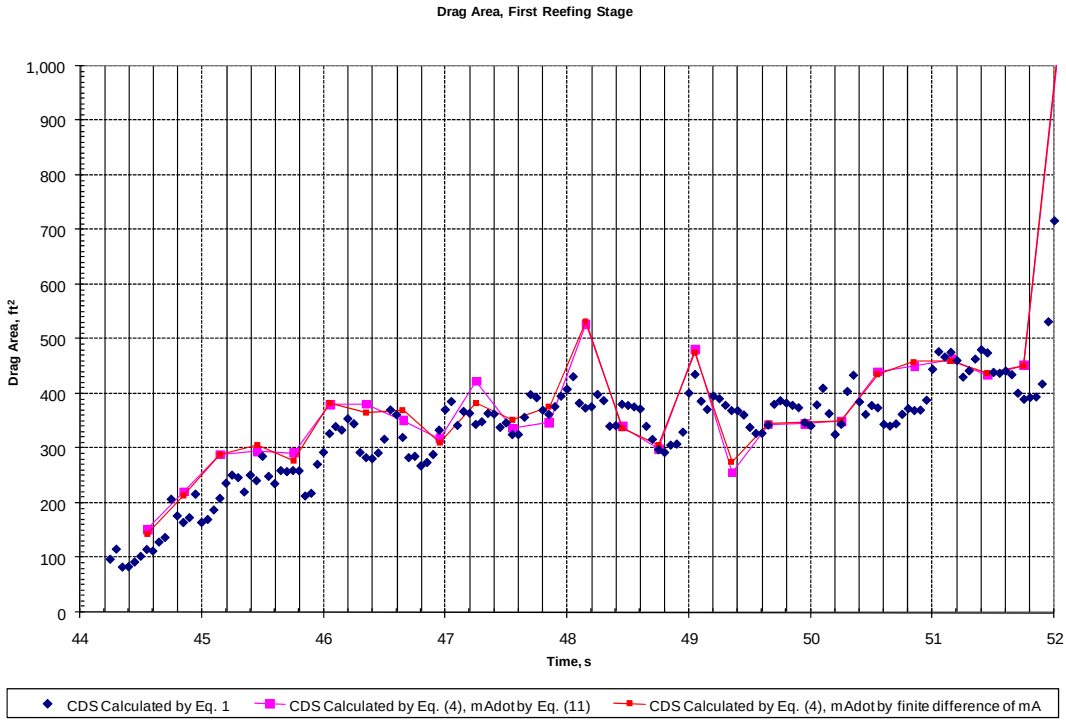

Figure 12. Drag area time history during the first reefing stage.

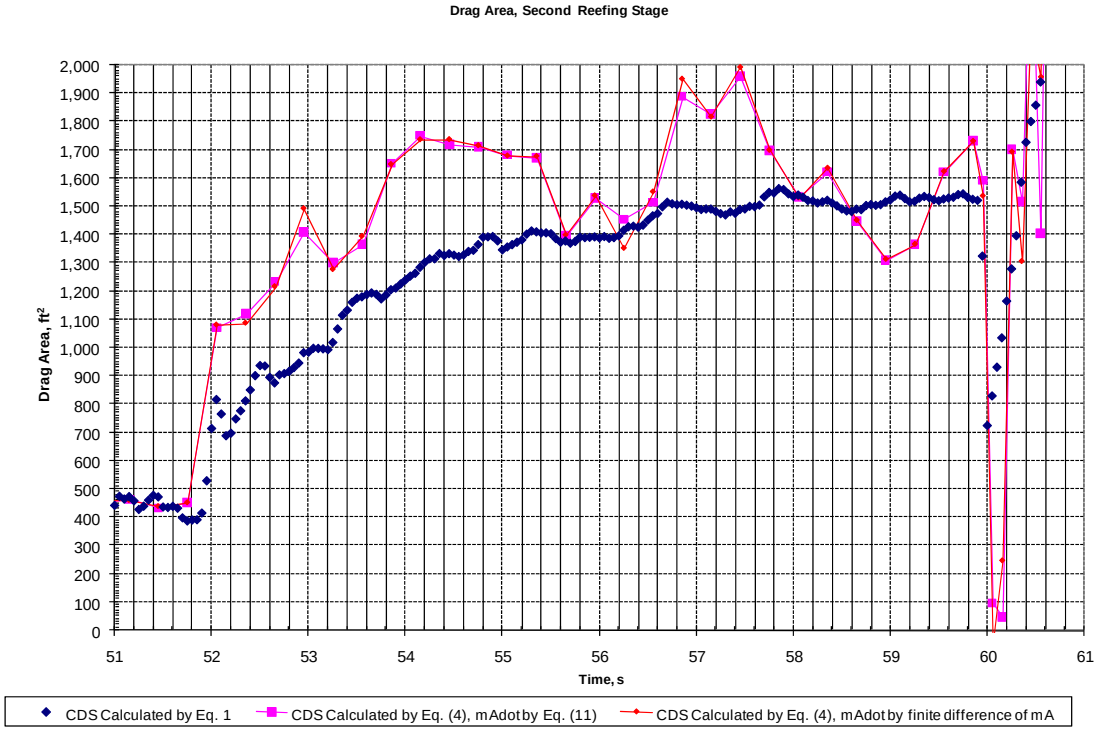

Figure 13. Drag area time history during the second reefing stage.

The value of the drag area as represented by these figures reflects the values of added mass in that the growth in drag area is similar to the growth in the mass values. Figures 12 and 13 indicate that the drag area values calculated by Eq. (1) and Eq. (4) are equivalent during the first reefing stage and nearly equivalent during the second reefing

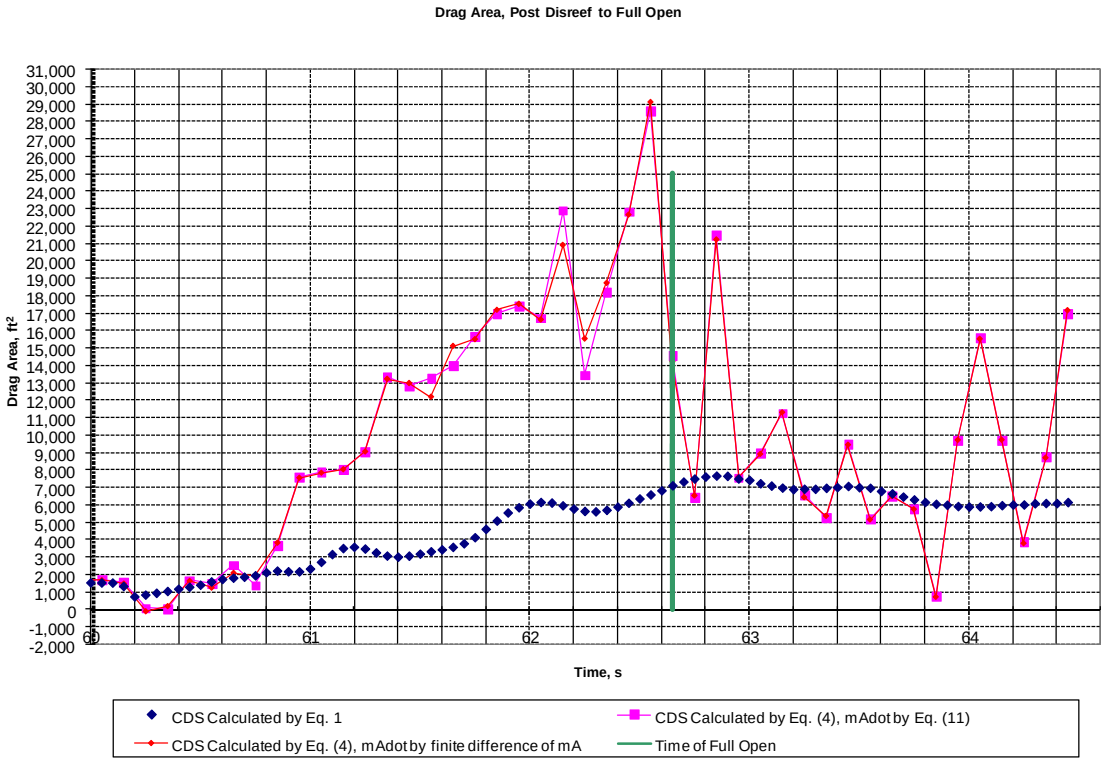

Figure 14. Drag area time history during the second reefing stage.

stage, whereas Fig. 14 suggests that the drag area values calculated by the two equations are significantly different during the period of canopy growth from disreef from the second stage to full open. As one would expect from an examination of Eqs. (1) and (4) drag area values established by equation (4) reach a higher maximum with a significantly higher growth rate as indicated in Fig. 14. This figure also indicates that the drag area calculated by Eq. (4) decreases to the same value as the drag area calculated by Eq. (1) for a period of 0.8 s beginning at 63 s. This behavior is due to the fact that beginning at 63 s the time derivative of added mass as well as acceleration is zero during this period.

VII. Conclusion

Based on the above results, there is no appreciable difference in the drag area growth characteristics of this class of parachute during portions of inflation where the size of the pressurized region of the canopy is relatively small – in the initial stages of inflation. However, there is evidence (Fig. 14) that the drag area is significantly larger when it is formulated as Eq. (4) versus Eq. (1), as one would expect, in the latter part of inflation when the size of the canopy reaches becomes relatively large causing values of added mass and change in added mass rate with respect to become appreciably large in turn influencing the drag area value.

The last observation in the previous section – the behavior of the drag area at points when $\dot{m}_A$ and acceleration are zero – is an illustration of the limitation of the approximation of the value of drag area given by Eq. (1) when the parachute is inflating and when it is fully inflated during periods of acceleration or deceleration due to fluctuations in elastic forces in the riser.

The difference in the two drag areas suggests that inputs to parachute performance computer models of representative drag area profiles as polynomial expressions of time and filling time based on drag area profiles determined by Eq. (1) as opposed to Eq. (4) will result in simulations based on Eq. (1) predicting lower opening forces than simulations based on Eq. (4) with peak forces possibly occurring at different points during inflation. In

addition the type of polynomial expression that could describe the drag area growth given by Eq. (1) -- during the full open stage of inflation -- could not describe the drag area growth as given by Eq. (4). For example

$$C_D S = (C_D S)_{FO} \left\lfloor \frac{(t - t_{FO})}{(t_{FO} - t_{IS})} \right\rfloor^N \tag{12}$$

which is a modification of Equation 7-28 from Ref. 6, where t refers to time and the subscripts FO and IS refer to full open and inflation start, respectively, could approximate the drag area growth during the third stage of inflation very well by varying the exponent, N. However, this expression could not approximate the drag area growth of Eq. (4) because of the overshoot of the full open value and the subsequent return to the full open value at 63 s.

At this point the limitations of the analysis presented in this paper should be mentioned. First, an examination of Figs. 2 -3 indicates that during the third stage of inflation that the velocity of the parachute is not aligned with its axis of symmetry and that the velocity is changing with time. This requires that additional components of the apparent mass tensor be included in formulation of the drag area growth. It also suggests that although a deviation is to be expected, the deviation in values of the drag area calculated using Eq. (1) and values calculated by Eq. (4) may not be as high as indicated by Fig. 14.

A logical extension of the work of this paper would be to formulate the drag area growth taking into account apparent mass terms resulting from all components of velocities and rotations for an approximating ellipsoid that is symmetrical about all three of its body fixed planes.

Appendix

This appendix provides a brief discussion of apparent mass and its derivation as used in this paper.

A. The kinetic energy of the fluid and the apparent mass[2, 4, 5.]

The kinetic energy of the fluid flow around the ellipsoid representing the inflating parachute at any time can be expressed as

$$T = \frac{1}{2}\rho \int_V u_i u_i dV \tag{13}$$

where i=1, 2, 3 indicate the three translation velocities, $u_i u_i$ is a shorthand notation meaning

$$u_1 u_1 + u_2 u_2 + u_3 u_3, \tag{14}$$

and, *V*, is the entire domain of the fluid in the continuous region between the surface of the body and the locus of points where the fluid velocity is equal to the freestream velocity. Eq. (13) may be written as

$$T = \frac{1}{2}\rho \int_V \frac{u_i}{U}\frac{u_i}{U} dV U^2 \tag{15}$$

because the change in fluid velocity is proportional to the freestream velocity or the body velocity, i.e. u_i changes by the same proportion that U changes. When the velocity of the body changes there is an attendant change in the kinetic energy of the fluid which is expressed by

$$-FU = \frac{dT}{dt} \tag{16}$$

where F is the force felt by the body, or the force on the body required to change the momentum of the fluid. The above expression is equivalent to

$$F = -\rho I \frac{dU}{dt} \tag{17}$$

if

$$I = \int_V \frac{u_i}{U} \frac{u_i}{U} dV \tag{18}$$

and I remains constant because the flow pattern does not change.

Because the above equation is analogous to $F = ma$, the force felt by the body when changing the momentum of the fluid, the product ρI is considered the apparent mass.

In the case of solid bodies moving through a fluid this expression may be called the added mass. However, in the case of parachutes, which are not solid bodies and capture air inside the canopy, the included mass is added to the apparent mass and this sum is called the added mass as stated previously.

The above formulations are suitable for simple rectilinear motion where only one direction is considered and a force applied to the body in one direction results in acceleration only in the same direction. In the general case, a force on the body may result in acceleration in another direction; there will be an induced acceleration in three translation coordinates and three rotation coordinates. For the apparent mass formulation to account for these induced accelerations, the apparent mass must be a matrix as in the following

$$F_i = -M_{ij} A_j \text{ [§]} \tag{19}$$

where F_i is a force on the body in the ith direction due to the change in the kinetic energy of the fluid in the jth direction and A_j -- with j=1, 2, 3 representing the three translation accelerations and with j=4, 5, 6 representing the three rotational accelerations – is the induced acceleration in the six possible induced acceleration directions. M_{ij} is the apparent mass matrix. If the induced accelerations are superposable, then the total induced velocity is the sum of the individual components of velocity of the fluid caused by each component of the body velocity. If the individual components of fluid flow are superposable, then the induced velocities due to motion of the body in each of its components can be summed as

$$u_i = u_{ij} U_j \tag{20}$$

where U_j is the body velocity, u_{ij} is the fluid velocity in the *i* component caused by the body velocity in the *j* component. A substitution of Eq. (19) into Eq. (12) allows the kinetic energy of the fluid to be expressed as

$$T = \frac{1}{2} A_{jk} U_j U_k \tag{21}$$

where

[§] See Ref. 5 which also indicates the moment of inertia tensor is added to the added to the apparent mass tensor of Eq. (19) to get the complete set of forces on the body.

$$A_{jk} = \rho \int_V u_{ij} u_{ik} \, dV \tag{22}$$

which is equal to the M_{ij} of Eq. (19).

B. The apparent mass in terms of the velocity potential[2, 5]

With substitution of

$$u_{ij} = \frac{\partial \phi_j}{\partial x_i} \tag{23}$$

and

$$u_{ik} = \frac{\partial \phi_k}{\partial x_i} \tag{24}$$

into Eq. (22) and application of Green's Theorem as done in Ref. 5 allows transformation of the volume integral of Eq. (22) into the following surface integral

$$A_{jk} = \rho \int_S \phi_j \frac{\partial \phi_k}{\partial n} \, dS \tag{25}$$

Solution of six velocity potentials, one due to motion of the body in each of its coordinates, allows the evaluation of each of the thirty-six components of the apparent mass matrix of Eq. (19).

C. Solution of the required velocity potentials[4]

Of the thirty-six elements of the apparent mass matrix, only the six diagonal elements need to be calculated for a body that is symmetrical about all three planes – i.e. the body is symmetrical about the $x_1 = 0$, $x_2 = 0$, $x_3 = 0$ planes. As a further simplification, if the body is moving only in one direction which is parallel to one of its axes, then the only the apparent mass component that needs to be calculated is the one related to the velocity potential of the fluid velocity caused by the body motion in that direction. In the case of a parachute motion with a body coordinate system in which the x_3 axis coincides with the parachute axis of symmetry, with a velocity only in its x_3 axis, the only element of the apparent mass tensor that needs to be calculated is

$$A_{33} = \rho \int_S \phi_3 \frac{\phi_3}{\partial n} \partial S \tag{26}$$

If the equation that describes the surface of the ellipsoid is

$$\frac{{x_1}^2}{a^2} + \frac{{x_2}^2}{b^2} + \frac{{x_3}^2}{c^2} = 1 \tag{27}$$

then the velocity potential is given by

$$\phi_3 = Cx_3 \int_{\lambda}^{\infty} \frac{d\lambda}{\left(c^2+\lambda\right)\sqrt{\left(a^2+\lambda\right)\left(b^2+\lambda\right)\left(c^2+\lambda\right)}} \tag{28}$$

where

$$C = \frac{abc}{2-\alpha_0} U_3 \tag{29}$$

where

$$\alpha_0 = abc \int_{0}^{\infty} \frac{d\lambda}{\left(c^2+\lambda\right)\sqrt{\left(a^2+\lambda\right)\left(b^2+\lambda\right)\left(c^2+\lambda\right)}} \tag{30}$$

So

$$\phi_3 = \frac{abc}{2-\alpha_0} U_3 x_3 \int_{\lambda}^{\infty} \frac{d\lambda}{\left(c^2+\lambda\right)\sqrt{\left(a^2+\lambda\right)\left(b^2+\lambda\right)\left(c^2+\lambda\right)}} \tag{31}$$

$$\phi_3 = \frac{\alpha_0 U_3 x_3}{2-\alpha_0} \tag{32}$$

Substituting Eq. (32) into Eq. (26) and applying the boundary condition, $\frac{\partial \phi}{\partial n} = U_3 \cos\theta_{x_3}$, results in

$$A_{33} = \rho \int_S \left(\frac{\alpha_0 U_3 x_3}{2-\alpha_0} \right) U_3 \cos\theta_{x_3} \partial S = \frac{\rho \alpha_0 {U_3}^2}{2-\alpha_0} \int_S x_3 \cos\theta_{x_3} \partial S \tag{33}$$

The integral $\int_S x_3 \cos\theta_{x_3} \partial S$ is a projection of an infinitesimal area of the ellipsoid surface onto the $x_3 = 0$ plane, making the integral equal to the volume of the ellipsoid, such that

$$A_{33} = \frac{\rho \alpha_0}{2-\alpha_0} \frac{4}{3} \pi abc \tag{34}$$

where α_0 is given by Eq. 30. This value is the apparent mass of a symmetrical parachute moving along its axis of symmetry.

Acknowledgments

Scott Roland, Vladimir Drozd, Dave Peterson, Randy Olmstead, Leo Lichodziejewski, Ben Tutt, Bob Shiley, Robert Sinclair, Tony Taylor, Judy Hansen.

References

[1]Taylor, A. and Murphy, E, "The DCLDYN Parachute Inflation and Trajectory and Analysis Tool – An Overview," 18th AIAA Aerodynamic Decelerator Systems Technology Conference and Seminar, AIAA, Reston, VA, 2005, pp. 234-242.

[2]Brennen, C. E., "A Review of Added Mass and Fluid Inertial Forces," Naval Civil Engineering Laboratory, Rept. N62583-81-MR-554, Port Hueneme, CA, Jan. 1982.

[3] Yavus, Tahir, "Theoretical Evaluations of Apparent Masses for Certain Classes of Bodies in Frictionless Fluid," Erciyes Universitesi, Dergisi, Turkey, 1986 (unpublished).

[4]Milne-Thomson, L.M., *Theoretical Hydrodynamics*, 5th ed, Dover, New York, 1968, pp. 530-535.

[5]Yih, C-S, *Fluid Dynamics: A Concise Introduction to the Subject*, 5th ed, McGraw Hill, New York, 1969, pp. 7, 86, 100, 99-103.

[6]Ewing, E. G., Bixby, H. W., and Knacke, T. W., "Recovery Systems Design Guide," Air Force Flight Dynamics Laboratory., Technical Rept. AFFDL-TR-78-151, Wright-Patterson Air Force Base, OH, Dec. 1978.